Prospects for SUSY at Future Linear e^+e^- Colliders

Keisuke FUJII

National Laboratory for High Energy Physics (KEK)
1-1 Oho, Tsukuba, Ibaraki 305, Japan

Abstract

Prospects for SUSY at future linear e^+e^- colliders are discussed from experimental point of view. It is pointed out that the first SUSY particle alone will provide a lot of information on SUSY breaking parameters, thereby setting the energy for the discovery of the next. The experimental procedures to determine the masses and mixings of SUSY particles through the measurements of various differential cross sections are explained, where the power of polarized electron beam is stressed. The implications of the so determined SUSY breaking parameters are discussed in relation to the GUT scale physics.

Talk presented at SUSY95,
May 15-19, 1995, Paris, France

1 Introduction

The existence of at least one light neutral Higgs boson is one of the most important predictions of low energy supersymmetry (SUSY). Its discovery alone is, however, not enough to prove the supersymmetry. It is definitely necessary to find *at least* one supersymmetric particle (sparticle) to show that there is indeed SUSY in nature. This qualitative confirmation of the supersymmetric part of the Lagrangian ($\mathcal{L}_{SUSY}$) is only an appetizer at a future linear e^+e^- collider. The supersymmetry breaking (sbreaking) part ($\mathcal{L}_{sbreaking}$), which determines masses and mixings of sparticles is the main dish, since it is believed to be determined by GUT or Planck scale physics. As illustrated in Fig. 1, experimentalists' tasks can, therefore, be summarized as follows: (1) search for a sparticle to qualitatively prove the existence of $\mathcal{L}_{SUSY}$, and (2) determine masses and mixings of sparticles through the measurements of various differential cross sections, thereby testing SUSY quantitatively and uncovering the structure of $\mathcal{L}_{sbreaking}$.

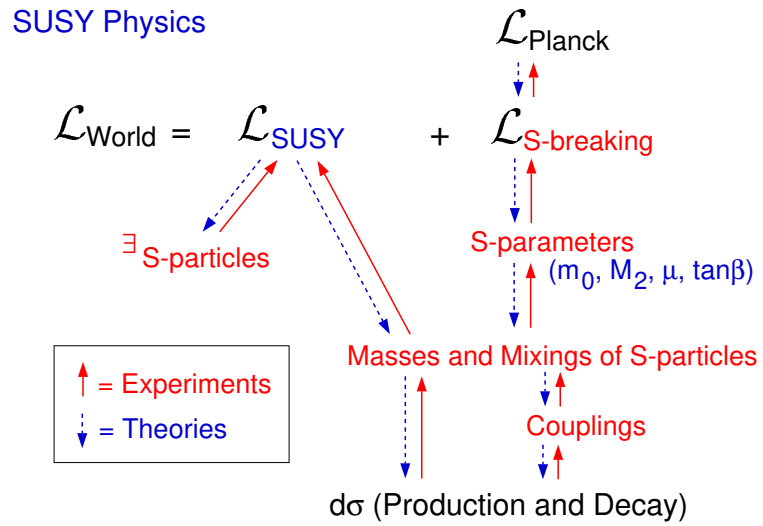

Figure 1: A schematic diagram showing the relation between the SUSY studies at a future linear e^+e^- collider and GUT or Planck scale physics. The dashed arrows indicate the logical flow of theoretical implications, while the solid arrows show that of experimental inputs.

In this talk, I will demonstrate a typical SUSY scenario at a future linear e^+e^- collider.

2 SUSY Study Scenario

Extensive studies have been carried out for SUSY searches at future linear colliders[1]. General conclusion from these studies is that as long as the mass difference between a target sparticle and the lightest SUSY particle (LSP) is not too small, say greater than 20 GeV, its detection at next generation linear e^+e^- colliders is easy. Because of this and time limitation, we are going to skip details of event selection. Instead, we will concentrate on what we can learn from sparticles to be found.

We take a sample parameter set:

$$(m_0, M_2, \mu, \tan\beta) = (70\ \text{GeV}, 250\ \text{GeV}, 400\ \text{GeV}, 2) \tag{1}$$

unless otherwise stated. Using this sample case, I will show you how a typical SUSY scenario goes at the linear collider[2]. This parameter set gives the following sparticle mass spectrum:

$$m_{\tilde{\chi}_1^0} = 118,\ m_{\tilde{\chi}_2^0} = 222,\ m_{\tilde{\chi}_1^\pm} = 220,\ m_{\tilde{l}_R} = 142,\ m_{\tilde{l}_L} = 236,\ m_{\tilde{\nu}_L} = 227\ \text{GeV}. \tag{2}$$

Thus our first SUSY particle (FSP) will be the right-handed sleptons pair-produced in e^+e^- collisions.

2.1 Study of $\tilde{l}^{\pm}_{R}(l \neq \tau)$

Since a right-handed slepton decays directly into a lepton plus an LSP, the signal to look for is an acoplanar lepton pair: $e^+e^- \to \tilde{l}^+_R\tilde{l}^-_R \to l^+\tilde{\chi}^0_1 l^-\tilde{\chi}^0_1$. On the other hand, the background to this reaction is standard model (SM) processes with neutrinos which mimic the LSP. The key point here is the power of a highly polarized electron beam available only at linear colliders. For instance, you can eliminate the largest SM background ($e^+e^- \to W^+W^-$ with $W \to l\nu$) very effectively, using a right-handed electron beam: the transverse W-pair production vanishes in the symmetry limit since the s-channel diagram involves a W^0 and the t-channel diagram exchanges a ν_e, both of which only couple to left-handed electrons. On the other hand, the signal cross section will be enhanced because of the weak hypercharge difference between e^-_L and e^-_R: $\sigma_R = 4\sigma_L$ in the symmetry limit. We can see this clearly in Fig. 2, which plots the acoplanarity distributions for smuon pair production with and without the right-handed electron beam. The requirement of $\theta_A > 30°$ eliminates the background to a negligible level,

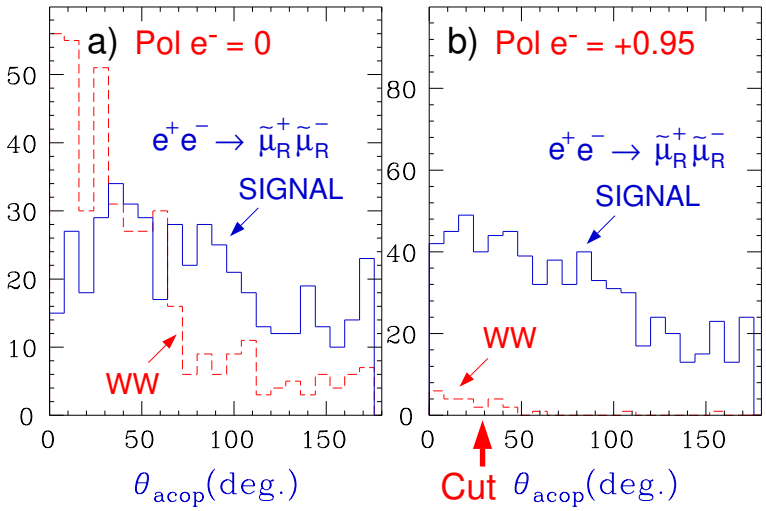

Figure 2: Examples of acoplanarity distributions for smuon pair productions with (a) an unpolarized beam and (b) a 95 %-right-handed polarized beam. The Monte Carlo data correspond to an integrated luminosity of 20 fb^{-1} at $\sqrt{s}$ = 350 GeV. The solid histograms are for the signal events, while the dashed histograms are the background from W^+W^- productions.

providing us with a very clean sample for precision studies.

Using this clean sample, we can determine the masses of the LSP and the right-handed slepton through the measurement of the final-state lepton energy distribution (see Fig. 3-a)): the end points of this distribution are kinematically fixed by the LSP and the slepton masses. A two-parameter fit to this distribution gives a contour plot shown in Fig. 3-b), which tells us that we can determine these masses to a 1% level.

With the right-handed selectron and smuon masses determined this way, we can make a very important test of the sbreaking sector, which is a test of generation independence of sfermion masses. The hidden sector SUSY breaking implies the universality of scalar masses at the GUT scale, which leads to the mass degeneracy of the first and the second generations. Fig. 4 is an example of the test of the generation independence, demonstrating potential precision available at the future linear collider.

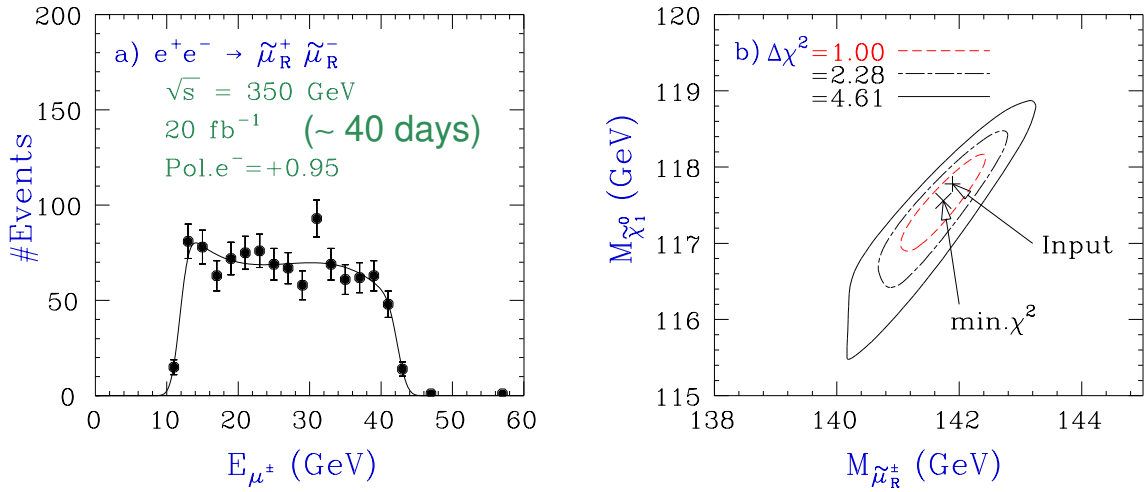

Figure 3: (a) Energy distribution of muons from smuon decays for the same Monte Carlo parameters as with Fig.2-b). The solid line corresponds to the best fit curve, letting $m_{\tilde{\mu}_R}$ and $m_{\tilde{\chi}^0_1}$ move freely. (b) Contours in the $m_{\tilde{\mu}_R}$-$m_{\tilde{\chi}^0_1}$ plane obtained from the fit to the energy distribution.

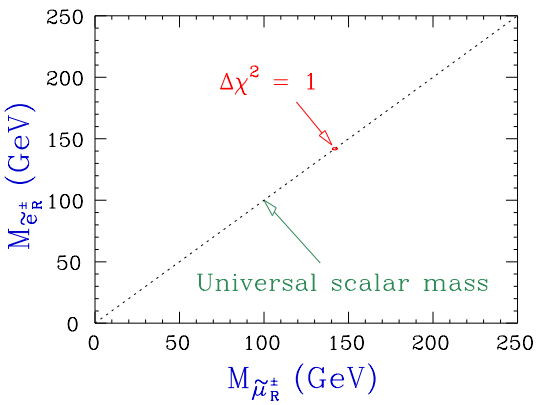

Figure 4: The expected $\Delta\chi^2 = 1$ contour in the $m_{\tilde{\mu}_R}$-$m_{\tilde{e}_R}$ plane.

Now that we know the masses of the LSP and the sleptons, we can solve kinematics up to 2-fold ambiguities. Fig. 5-a) plots the two solutions for the cosine of the smuon production angle. Comparison of this with the corresponding generated one (histogram) suggests that the wrong solution makes a flat background. After the background subtraction, we get the plot in Fig. 5-b), which shows a $\sin^2\theta$ distribution characteristic of s-channel pair productions of a spinless particle. In this way we can confirm that our smuon is really a scalar particle.

On the other hand, the right-handed selectron pair production has t-channel neutralino-exchange diagrams in addition. Notice that only their bino ($\tilde{B}$) components contribute here, which will produce a forward peak if significant. Figs. 5-c) and -d) are similar plots to Figs. 5-a) and -b) for the right-handed selectron pair production. The forward peak indicates that our LSP is bino-dominant.

2.2 $\tilde{\tau}^\pm$ Study

As explained below, studies of stau decays provide another handle to uncover the nature of the LSP through the measurement of the final state tau polarization [3]. For simplicity, let us assume that $\tilde{\tau}_L$-$\tilde{\tau}_R$ mixing is negligible and the lighter stau is essentially $\tilde{\tau}_R$. If the LSP is bino-dominant ($\tilde{\chi}^0_1 \simeq \tilde{B}$), the final-state tau will be right-handed ($\tilde{\tau}_R^- \to \tau_R^- \tilde{\chi}^0_1$), since the $\tilde{\tau}\tilde{\chi}^0_1\tau$

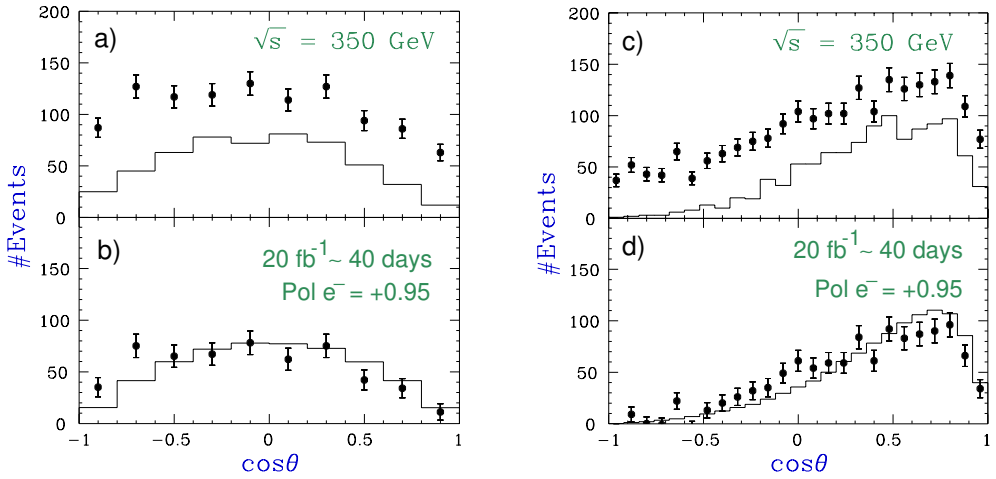

Figure 5: (a) Production angle distribution of $\tilde{\mu}_R^-$ with respect to the electron beam axis. The points with error bars are the distribution of the two solutions reconstructed from the selected sample corresponding to Fig. 3-a). The histogram is the generated $\cos\theta$ distribution for the selected sample. (b) Production angle distribution after the background subtraction compared with the scaled generated distribution before selection cuts. No acceptance correction is applied to the reconstructed distribution. (c) and (d) are similar plots to (a) and (b) for $e^+e^- \to \tilde{e}_R^+\tilde{e}_R^-$.

coupling stems from the gauge coupling, which is chirality-conserving. On the other hand, if the LSP is higgsino-dominant ($\tilde{\chi}_1^0 \simeq \tilde{H}_1^0$), the $\tilde{\tau}\tilde{\chi}_1^0\tau$ coupling will be of Yukawa type and chirality-flipping, thereby resulting in a left-handed tau in the final state. We can thus determine the nature of the LSP by measuring the final-state tau polarization. Figs. 6-a) and -b) shows examples of such a measurement for the bino- and higgsino-dominant cases, respectively. It should be emphasized that this measurement is unique to the stau decays. From the figures, we can see that $\Delta P_\tau \simeq 0.1$ is quite feasible, given an integrated luminosity of 100 fb^{-1}.

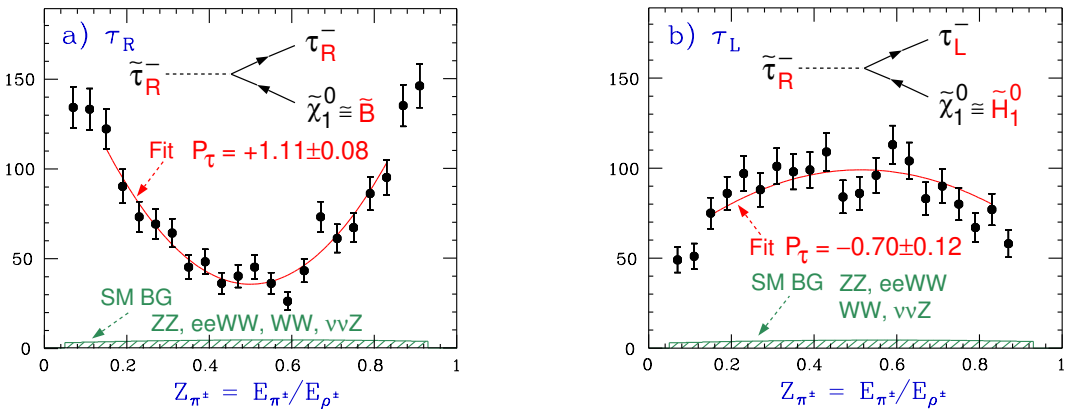

Figure 6: Distributions of the $\pi^\pm$ energy fraction with respect to the energy of the $\rho^\pm$ from $\tau \to \nu_\tau\rho$ decays for (a) bino-dominant and (b) higgsino-dominant LSP cases. The points with error bars are the Monte Carlo data corresponding to 100 fb^{-1} with $P_{e^-} = +0.95$ at $\sqrt{s} = 500$ GeV, where $m_{\tilde{\tau}} = 150$ GeV, $m_{\tilde{\chi}_1^0} = 100$ GeV, and $\sigma_{\tilde{\tau}\tilde{\tau}} = 100$ fb are assumed. The shaded histograms are the expected standard-model backgrounds from $e^+e^- \to ZZ, W^+W^-$, $e^+e^-W^+W^-$, and $\nu\bar{\nu}Z$.

2.3 Study of $\tilde{\chi}_1^\pm$

From the slepton studies, we can determine the mass of the LSP($\tilde{\chi}_1^0$) to better than 1 %. From this we can set an upper limit on the lighter chargino mass, assuming the GUT relation among

the gaugino mass parameters. This upper limit corresponds to the gaugino-dominant case ($m_{\tilde{\chi}_1^\pm} \simeq 2 \times m_{\tilde{\chi}_1^0}$), while the LSP and the lighter chargino will be almost mass-degenerate in the higgsino-dominant case. The upper limit is plotted in Fig. 7 as a function of the LSP mass.

We thus set our center of mass energy just above $4 \times m_{LSP}$ and look for $\tilde{\chi}_1^\pm$ pair productions. In our sample case, the chargino decays into a real W and an LSP ($\tilde{\chi}_1^\pm \to W^\pm \tilde{\chi}_1^0$). The signal to look for will thus be an acoplanar W pair in 4-jet final states. Fig. 8 shows the acoplanarity angle distribution for the signal events (solid histogram) together with major standard-model backgrounds. A cut at $\theta_A = 30°$ will give us a fairly clean sample for precision

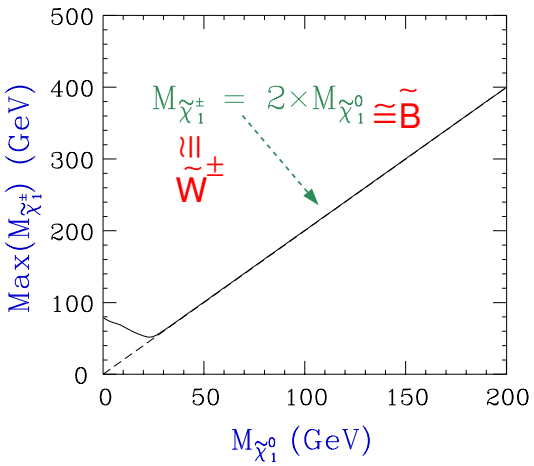

Figure 7: Upper limit on the lighter chargino mass as a function of the LSP mass, assuming the GUT relation.

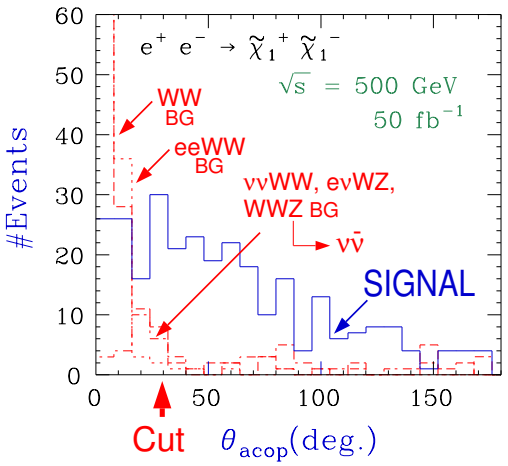

Figure 8: Acoplanarity angle distribution for $e^+e^- \to \tilde{\chi}_1^+\tilde{\chi}_1^-$ together with major standard-model backgrounds.

studies.

As we did to the sleptons, we can first use this clean sample to determine the chargino mass. Fig. 9-a) plots the expected energy distribution of the final-state W's from the chargino decays. The solid curve is the best-fit curve from a 2-parameter fit letting the $m_{\tilde{\chi}_1^\pm}$ and $m_{\tilde{\chi}_1^0}$ move freely. Notice that the fit includes the standard-model backgrounds shown as dashed, dot-dashed, and dotted curves, corresponding to those in Fig. 8. Fig. 9-b) is the resultant contour plot in the $m_{\tilde{\chi}_1^\pm}$-$m_{\tilde{\chi}_1^0}$ plane, which tells us that we can determine the chargino mass to $\Delta m_{\tilde{\chi}_1^\pm} \simeq 8$ GeV. If we use the LSP mass constraint from the slepton study, we can improve this to $\Delta m_{\tilde{\chi}_1^\pm} \simeq 5$ GeV.

Using the clean sample, we can also measure the production cross section. Notice that, for the right-handed electron beam, only higgsino components contribute to the chargino pair production in the symmetry limit, since the gauge boson exchanged in the s-channel is B ($U(1)_Y$ gauge boson), which does not couple to wino components. By measuring the production cross section for the right-handed electron beam, we can thus determine the composition of $\tilde{\chi}_1^\pm$.

We now know the LSP ($\tilde{\chi}_1^0$) and the chargino ($\tilde{\chi}_1^\pm$) masses, which constrain the chargino and neutralino mass matrices, the production cross section for $e^+e_R^- \to \tilde{e}_R^+\tilde{e}_R^-$, which depends on the bino component of the LSP, and the production cross section for $e^+e_R^- \to \tilde{\chi}_1^+\tilde{\chi}_1^-$, which provides information on the chargino composition. Combining these measurements together, we can carry out a global fit to determine sbreaking parameters: $(M_1, M_2, \mu, \tan\beta)$. Notice that we did not assume the GUT relation between M_1 and M_2 here, since this is what we want to test now. Fig. 10 is the result from such a global fit to Monte Carlo data generated with the GUT relation indicated as a dashed line. In this way, we can test the GUT relation.

So far, we have been assuming SUSY, being satisfied with a qualitative test of SUSY (the existence of a new particle consistent with sparticle interpretation). At this point, we can

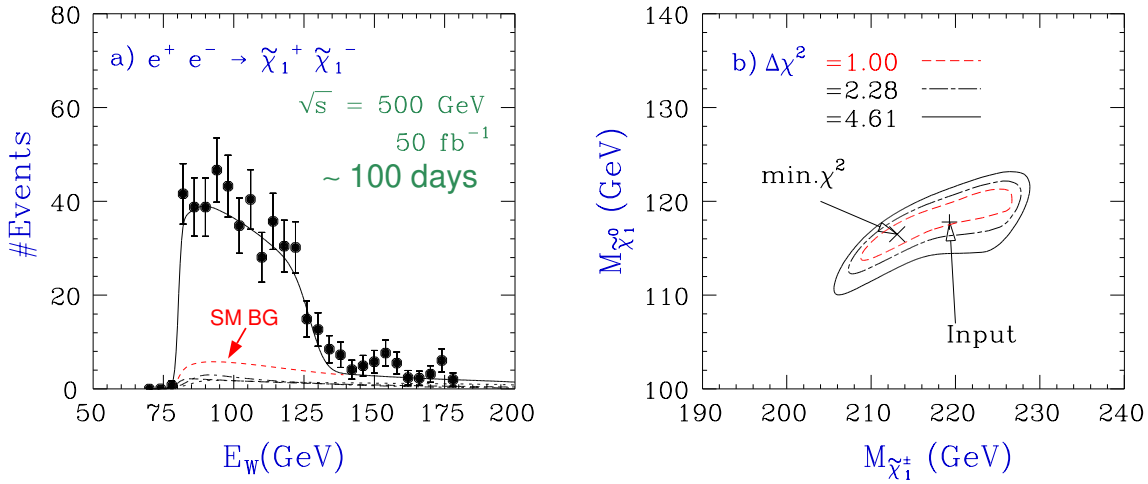

Figure 9: (a) Energy distribution of final-state W's from chargino decays: $\tilde{\chi}_1^\pm \to W^\pm \tilde{\chi}_1^0$ (points with error bars) for the sample shown in Fig. 8 after the acoplanarity angle cut at $\theta_A = 30°$. The solid curve is the best-fit curve to determine $m_{\tilde{\chi}_1^\pm}$ and $m_{\tilde{\chi}_1^0}$. The other curves correspond to the histograms in Fig. 8. (b) Resultant contours from the 2-parameter fit.

even try to test SUSY quantitatively[4]. In general SUSY relates mutually supersymmetric couplings: $e_L \tilde{W} \tilde{\nu}$ and $e_L W \nu$ for instance. This relation can be cast into the form $g = g^\chi$, where g represents the $SU(2)_L$ gauge coupling. For simplicity, let us consider a gaugino-dominant $\tilde{\chi}_1^\pm$ and assume that the chargino mixing is negligible. Then the free parameters that enter the differential cross section for a left-handed electron beam are essentially $m_{\tilde{\nu}}$ and g^χ, since we already know $m_{\tilde{\chi}_1^\pm}$. In order to determine these two unknown parameters, we can use the production cross section (σ_L) and the forward backward asymmetry (A_L^χ)[1] for the left-handed electron beam. Fig 11 shows the constraints from the σ_L and A_L^χ measurements on the two unknown parameters. The horizontal dotted line indicates the SUSY prediction.

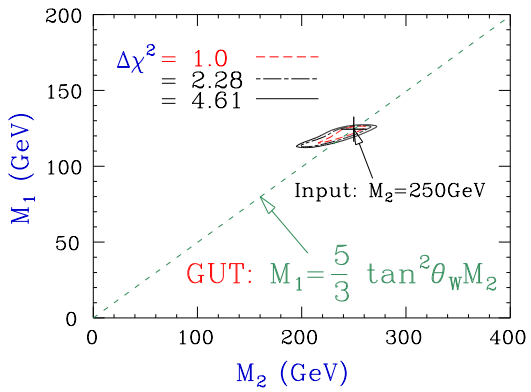

Figure 10: Constant χ^2 contours in the M_2-M_1 plane obtained from the global fit explained in the text. The dotted line shows the GUT relation.

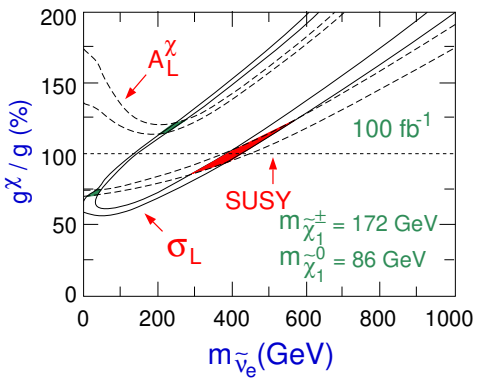

Figure 11: Constraints in the $m_{\tilde{\nu}}$-g^χ/g plane from σ_L and A_L^χ measurements with 100 fb^{-1}[4] for $(M_2, \mu, m_{\tilde{l}}, m_{\tilde{q}}) = (170, -500, 400, 700)$ GeV and $\tan\beta = 4$.

Once we are convinced with SUSY, we can tell the sneutrino mass from this figure. Using this and the following model-independent inequality

$$m^2_{\tilde{e}^\pm_L} \leq m^2_{\tilde{\nu}_e} + 0.77 m_Z^2, \tag{3}$$

[1]We cannot measure A^χ directly. There is, however, a strong correlation between the asymmetry of $\tilde{\chi}_1^-$ and that of W^-. We can measure the latter using lepton+2-jet final states.

we can set an upper limit on the left-handed selectron mass. Let us now look for the left-handed selectron in $e^+e^-_R \to \tilde{e}^+_L\tilde{e}^-_R$.

2.4 $\tilde{e}^{\pm}_L$ Study

The associate production of $\tilde{e}_L$ with $\tilde{e}_R$ proceeds via t-channel exchange of neutralinos, to which only the $\tilde{B}$ components contribute. The signal for this process is an acoplanar e^+e^- pair. When we use the right-handed electron beam to suppress standard-model backgrounds, the major background is our previous signal: $e^+e^-_R \to \tilde{e}^+_R\tilde{e}^-_R$. Notice that the use of the right-handed electron beam selects the e^+ in the final state as a carrier of the $\tilde{e}_L$ information. Fig. 12 plots the final-state electron energy against that of the positron, clearly demonstrating this fact. Projecting this to the E_{e^+} axis, we obtain the distribution shown in Fig. 13-a), from which we

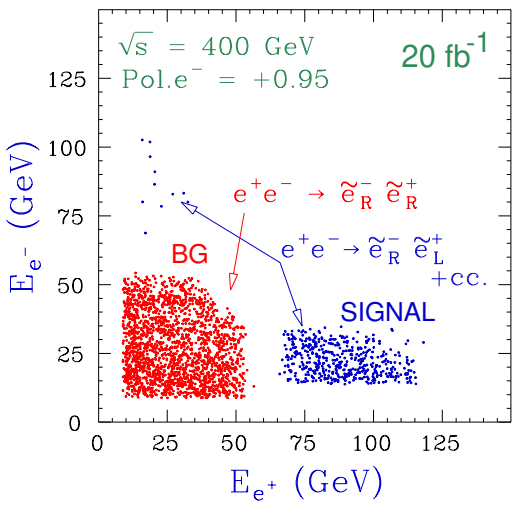

Figure 12: Distribution of final-state electron energy against that of the positron for $e^+e^-_R \to \tilde{e}^+_L\tilde{e}^-_R$ (signal) and $\tilde{e}^+_R\tilde{e}^-_R$ (background) at $\sqrt{s} = 400$ GeV with an integrated luminosity of 20 fb^{-1}.

can extract the sparticle masses as before. The contours from a 2-parameter fit are shown in

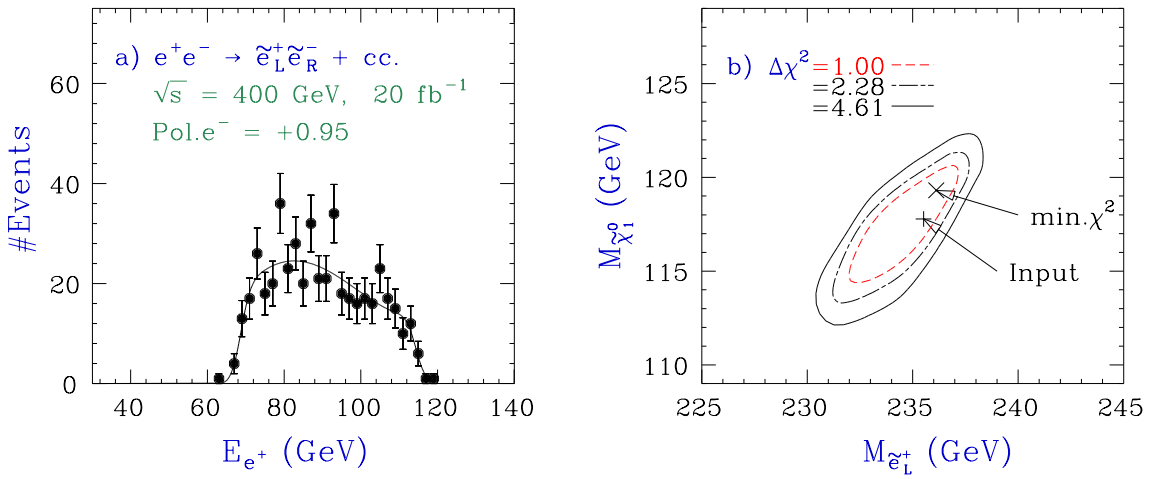

Figure 13: (a) Energy distribution of positrons from $\tilde{e}^+_L$ decays for the same Monte Carlo parameters as with Fig.12. The solid line corresponds to the best fit curve, letting $m_{\tilde{e}_L}$ and $m_{\tilde{\chi}^0_1}$ move freely. (b) Contours in the $m_{\tilde{e}_L}$-$m_{\tilde{\chi}^0_1}$ plane obtained from the fit to the energy distribution.

Fig. 13-b), which tells us that we can determine the left-handed selectron mass to an accuracy better than 1 %.

Knowing both the right-handed and left-handed selectron masses enables us to make another test of the universal scalar mass hypothesis. The squared mass difference of the right-

handed (belonging to $\mathbf{5}^*$) and left-handed (belonging to $\mathbf{10}$) selectrons is related through the following scalar mass formula:

$$m^2_{\tilde{e}_L} - m^2_{\tilde{e}_R} = m^2_{0(\mathbf{5})} - m^2_{0(\mathbf{10})} + 0.5M_2^2 - 0.04 \cdot m_Z^2 \cos 2\beta. \tag{4}$$

The universal scalar mass hypothesis implies the representation independence ($m_{0(\mathbf{5})} = m_{0(\mathbf{10})}$), which can be tested as shown in Fig. 14: compare the $\Delta\chi^2 = 1$ contour with the prediction of the universal scalar mass hypothesis (dashed lines for $\tan\beta = 0$ and 30). Notice that the last term ($\tan\beta$-dependent term) of the above equation is small and only makes slight difference, allowing us a clean test of the representation independence.

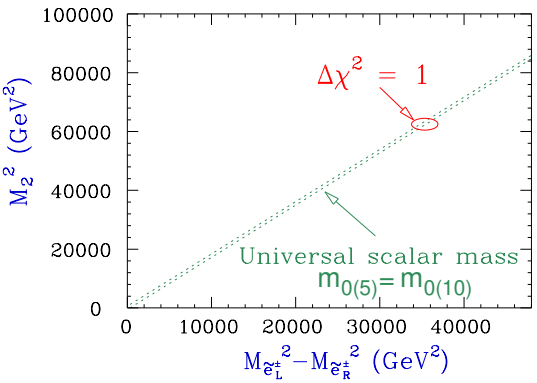

Figure 14: $\Delta\chi^2 = 1$ contour from the selectron mass measurements, compared with the prediction from the universal scalar mass hypothesis, indicated as dotted lines for $\tan\beta = 0$ and 30.

Once the GUT relation is confirmed and the universal scalar mass hypothesis is verified in the slepton sector, we can set, with confidence, the next target energy for $\tilde{q}$ pair production.

2.5 Study of $\tilde{\mathbf{q}}_{\mathbf{G}}(\mathbf{G} \neq \mathbf{3})$

A squark may decay into a quark plus an LSP or into a quark plus a chargino or heavier neutralino, depending on the sbreaking parameters. In the former case, the signal for squark pair production is an acoplanar 2-jet final state, while in the latter case it is a final state consisting of two jets plus one or two W/Z bosons from the cascade decays of the charginos or neutralinos, respectively. Potential backgrounds to this process thus include $e^+e^- \to W^+W^-$, $e^\pm \overset{(-)}{\nu}_e W^\mp$, $\nu\bar{\nu}Z$, $\tilde{\chi}_1^+\tilde{\chi}_1^-$, and $\tilde{\chi}_i^0\tilde{\chi}_j^0$. Notice that the 2-jet systems in the final states of these background processes are all from $W^{(*)}/Z^{(*)}$'s, thereby having invariant masses smaller than 100 GeV. We can therefore very effectively eliminate them by requiring $m_{q\bar{q}} > 100$ GeV, together with usual acoplanar 2-jet selection criteria like $\not{p}_T > 35$ GeV, and $\theta_A > 30°$. We can thus use both e_L^- and e_R^- beams without suffering from these would-be serious backgrounds. It should also be emphasized that the chirality selection of the final-state squarks works better than the slepton case: $\sigma_R(\tilde{q}_R\bar{\tilde{q}}_R) : \sigma_R(\tilde{q}_L\bar{\tilde{q}}_L) \simeq \sigma_L(\tilde{q}_L\bar{\tilde{q}}_L) : \sigma_L(\tilde{q}_R\bar{\tilde{q}}_R) \simeq 9 : 1$, if $m_{\tilde{q}_L} \simeq m_{\tilde{q}_R}$. By controlling the electron beam polarization, we can thus select the chirality of the final-state squarks and, consequently, study their properties separately. Let us first consider the mass determination in the case of the direct decay. In this case, we can use the end-point method as with $\tilde{l}^\pm$ and $\tilde{\chi}_1^\pm$. There is, however, a better quantity called minimum squark mass ($m_{\tilde{q}}^{min}$)[5]. defined by

$$\left(m_{\tilde{q}}^{min}\right)^2 = E_{beam}^2 - |\mathbf{p}_1|^2_{max} = E_{beam}^2 - |\mathbf{p}_2|^2 - |\mathbf{p}_3|^2 + 2|\mathbf{p}_2||\mathbf{p}_3|\cos(\delta+\gamma), \tag{5}$$

where the momenta and angles are defined in Fig. 15. Notice that the two angles δ and γ and the magnitude of the LSP momentum are calculable, provided that the LSP mass is known. Notice also that $m_{\tilde{q}}^{min}$ makes use of the information contained in the relative configuration of

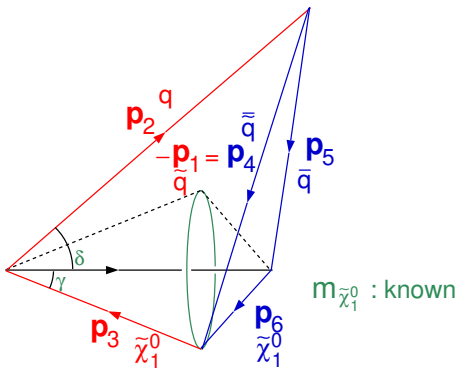

Figure 15: Definitions of the momenta and angles used to define the minimum squark mass. The LSP mass is assumed to be known precisely.

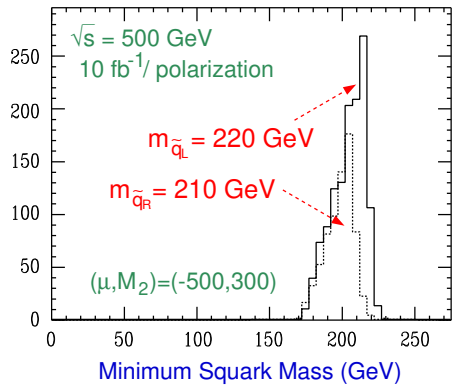

Figure 16: Expected $m_{\tilde{q}}^{min}$ distributions for left- and right-handed squarks cited from Ref.[5].

the final-state q and $\bar{q}$ unlike in the end-point method. Fig. 16 shows an example of expected $m_{\tilde{q}}^{min}$ distributions for parameters shown in the figure. We can see that the Jacobian peaks are good measures of the squark masses and allow their precision measurements: $\Delta m_{\tilde{q}} \simeq 1$ GeV at the 95 % confidence level.

If cascade decays dominate the direct decay, we select final-states with two jets plus leptons and pretent to be blind to the leptons. Notice that these leptons are end-products of the chargino ($\tilde{\chi}_1^{\pm}$) or heavier neutralino ($\tilde{\chi}_2^0$), whose masses are almost degenerate and presumably known from the earlier measurements. We can thus change the role of the LSP in the direct decay case by that of the chargino or second neutralino, by ignoring the final-state leptons. In this way, we can again calculate the minimum squark mass for each event and carry out the squark mass measurement at a 1 % level, provided that $m_{\tilde{\chi}_1^{\pm}}$ and $m_{\tilde{\chi}_1^0}$ are known.

3 Summary and Conclusion

We have quickly gone through a typical SUSY scenario at a future linear e^+e^- collider. Its main features can be summarized as follows. (1) The power of the polarized electron beam will be essential to selecting Feynman diagrams for both signal and background processes, thereby suppressing various backgrounds and sorting out sparticle mixings. (2) The first sparticle alone will provide us with enough information to set where to go for the next sparticle. (3) We can make precision measurements of various quantities from differential cross sections such as masses, mixing angles, and couplings, which allow us to test the key assumptions of the supergravity models such as GUT relations, the hidden-sector SUSY-breaking (universal scalar mass), etc.

We can conclude that the future linear e^+e^- collider will enable us to take a first realistic step towards the GUT/Planck scale physics, once a sparticle is found there.

Acknowledgements

The author wishes to thank all the members of the JLC working group for useful discussions and comments. In particular, S. Murayama, M. Nojiri, Y. Okada, T. Tsukamoto, M. Yamaguchi deserve special mention, since most of the materials presented here are based on the collaboration with them. The author is very grateful to J. Feng, K. Hikasa, T. Kon, M. Jimbo, and M. Peskin for valuable discussions. Finally the author would like to express his heartfelt gratitude to the workshop organizers for their efforts to make it so comfortable and

so fruitful.

References

[1] J. Grivaz, DESY 92-123B p663; R. Becker and C. Vander Velde, DESY 92-123C p457.

[2] T. Tsukamoto, K. Fujii, H. Murayama, M. Yamaguchi, and Y. Okada, Phys.Rev. D51 (1994) p3153.

[3] M. Nojiri, Phys.Rev. D51 (1995) p6281; M. Nojiri, K. Fujii, and T. Tsukamoto, in preparation.

[4] J. Feng, M. Peskin, H. Murayama, and X. Tata, Phys.Rev. D52 (1995) p1418.

[5] J. Feng and D. Finnell, Phys.Rev. D49 (1994) p2369.